JACS
JOURNAL OF THE AMERICAN CHEMICAL SOCIETY

Communication

pubs.acs.org/JACS

Cell Environment-Differentiated Self-Assembly of Nanofibers

Zhen Zheng,[†] Peiyao Chen,[†] Maolin Xie,[‡] Chengfan Wu,[†] Yufeng Luo,[†] Wentao Wang,[⊥] Jun Jiang,[‡] and Gaolin Liang*[,†]

CAS Key Laboratory of Soft Matter Chemistry, [†]Department of Chemistry and [⊥]Department of Polymer Science and Engineering and [‡]Hefei National Laboratory for Physical Sciences at the Microscale, Department of Chemical Physics, University of Science and Technology of China, 96 Jinzhai Road, Hefei, Anhui 230026, China

Supporting Information

ABSTRACT: Employing cellular environment for the self-assembly of supramolecular nanofibers for biological applications has been widely explored. But using one precursor to differentiate the extra- and intracellular environments to self-assemble into two different nanofibers remains challenging. With the knowledge that the extracellualr environment of some cancer cells contains large amounts of alkaline phosphatase (ALP) while their intracellular environment is glutathione (GSH)-abundant in mind, we rationally designed a precursor Cys(SEt)-Glu-Tyr(H_2PO_3)-Phe-Phe-Gly-CBT (**1**) that can efficiently yield amphiphilic **2** and **2-D** to self-assemble into two different nanofibers in hydrogels under the sequential treatment of ALP and GSH. We envision that, by employing a click condensation reaction, this work offers a platform for facilely postmodulation of supramolecular nanofibers, and the versatile precursor **1** could be used to kill two birds with one stone.

In terms of redox, the intracellular and extracellular environments of a mammalian cell are quite different. Generally, the intracellualr cytosol is a reducing environment, characterized by a ~ mM level of glutathione (GSH) content.[1,2] In the extracellular compartment, GSH is converted to GSH disulfide (i.e., GSSG) by cell membrane-bound oxidases, and thus the extracellular environment is generally viewed oxidative and redox inert.[3−5] As the most abundant cellular thiol, GSH is an essential endogenous detoxicant that plays a central role in cellular defense against toxins and free radicals.[6,7] Since abnormal levels of GSH are often linked to cancer, aging, heart problems, and other ailments, intracellular GSH could be used as an important clinical biomarker.[8,9] Recently, Yang et al. used intracellular GSH as the trigger to reduce the disulfide bound on the hydrogelator for the self-assembly of supramolecular nanofibers inside cells.[10−14]

Alkaline phosphatase (ALP) is an important and universal enzyme that is responsible for the cleavage of the phosphate groups from its substrate molecules, which are usually building blocks of DNA or proteins.[15] This process is important for intracellular signal transmission, protein activity regulation, etc.[16] Elevation of ALP level occurs in dynamic bone disease, diabetes, as well as human cancers.[17,18] Remarkably, due to its highly catalytic efficiency, ALP has been widely used to instruct the self-assembly of supramolecular nanofibers intracellularly.[19] Moreover, ALP was found highly expressed on the cell membrane or secreted out of some cancer cells (e.g., HeLa, MES-SA, and MES-SA/Dx5 cells).[20] Therefore, a few of ALP-instructed supramolecular nanofibers were reported to form in the pericellular spaces of these cancer cells.[21]

Inspired by the above poineering works, we intended to design a hydrogelator which can differentiate the cellular environments to self-assemble into two essentially different types of supramolecular nanofibers. To achieve this purpose, as illustrated in Figure 1, we rationally designed a 2-cyano-6-aminobenzothiazole (CBT)-based hydrogelator precursor, Cys(SEt)-Glu-Tyr(H_2PO_3)-Phe-Phe-Gly-CBT (**1**), which was proposed to sequentially response to ALP and GSH for hierarchical self-assemblies of two types of nanofibers, from extracellular to intracellular environments. Thus, **1** was designed to contain following components: A Tyr(H_2PO_3)-Phe-Phe motif, which is an essential part for the first-order ALP-instructed self-assembly,[22,23] a CBT motif (but not the commonly used naphthylene (Nap) or fluorenylmethyloxycarbonyl (Fmoc) group) to provide the intermolecular $\pi-\pi$ stacking in the first-order self-assembly, and a disulfided cysteine (Cys) motif for intracellular GSH-initiated condensation with the CBT motif,[24,25] which is responsible for the second-order nanofiber self-assembly. The reason we used CBT motif here is that recently we found luciferin (the condensation product of CBT and cysteine) and quinoxaline motifs were also good $\pi-\pi$ stacking suppliers for the self-assembly of supramolecular nanofibers.[26,27] As illustrated in Figure 1, in the extracellular environment, the enzyme ALP out of the cells or on the cell membrane catalytically dephosphorylates **1** to yield the hydrogelator Cys(SEt)-Glu-Tyr-Phe-Phe-Gly-CBT (**2**), which self-assembles into **nanofiber 2** in the pericellular space. Once endocytosed by the cell, the disulfide bond on the hydrogelator **2** will be reduced by intracellular GSH to expose the active 1,2-aminothiol group, which instantly condenses with the CBT motif on another molecule **2** to yield the cyclic dimer **2-D** (see Figure 2D for chemical structure). Then the amphiphilic **2-D** further self-assembles into **nanofiber 2-D** with enhanced mechanical strength compared to that of **nanofiber 2**. To validate the above mechanism, compound **2** (i.e., the ALP-cleaved product of **1**) was also synthesized.

We began the study with the syntheses of the precursor **1** and hydrogelator **2** (Schemes S1 and S2). The syntheses are simple and straightforward as follows: peptide sequence Boc-Cys(SEt)-Glu(OtBu)-Tyr(H_2PO_3)-Phe-Phe-Gly-OH (**1a**) with protec-

Received: July 4, 2016
Published: August 17, 2016

DOI: 10.1021/jacs.6b06903
J. Am. Chem. Soc. 2016, 138, 11128−11131

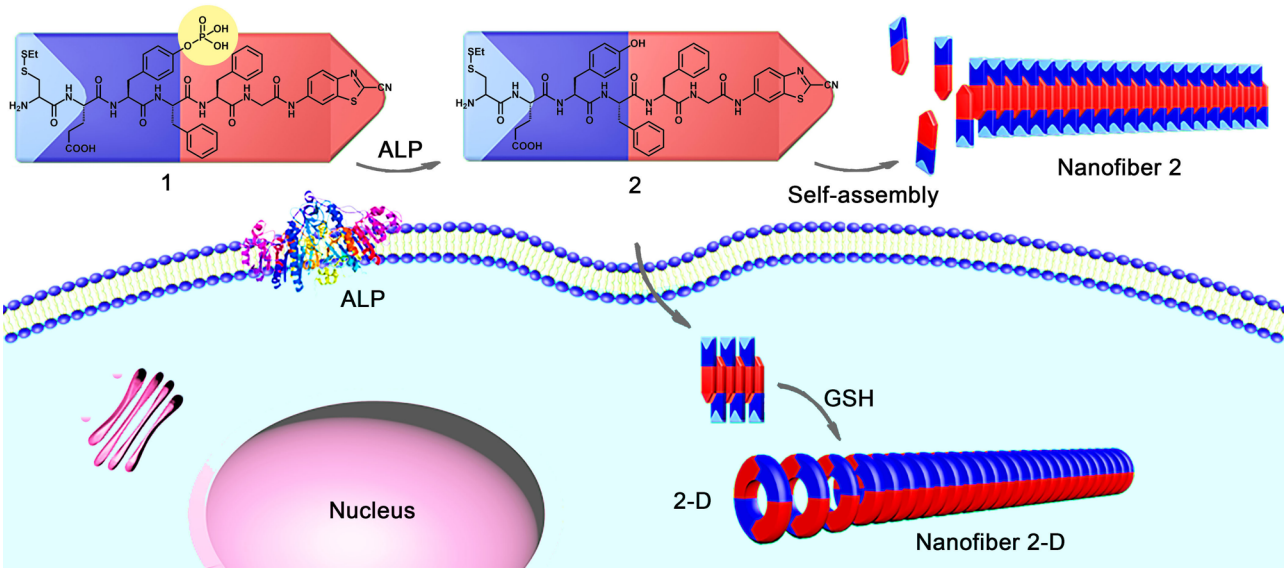

Figure 1. Schematic illustration of ALP-directed self-assembly of **1** into **nanofiber 2** in extracellular environment and GSH-controlled condensation of **2** to yield the cyclic amphiphilic dimer **2-D** which self-assembles into **nanofiber 2-D** in intracellular environment. Blue parts indicate the hydrophilic structures, and red parts indicate the hydrophobic structures.

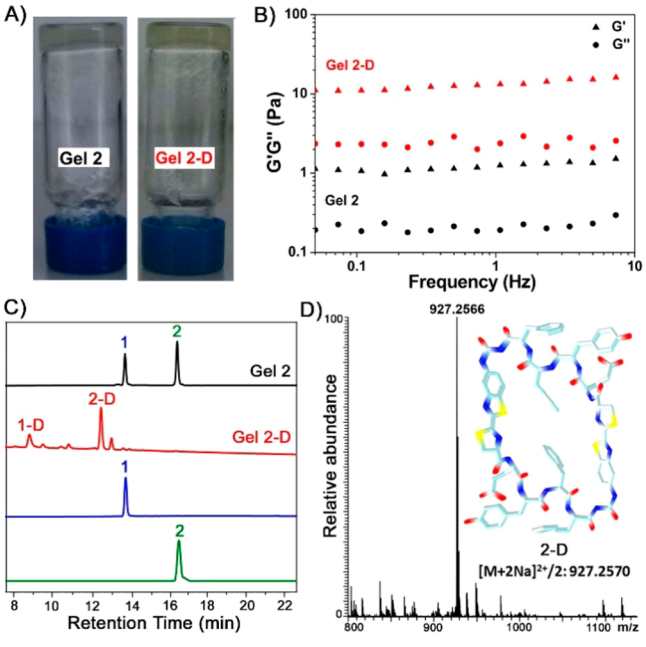

Figure 2. (A) Photographs of **gel 2** (left) and **gel 2-D** (right) at 1.0 wt %. (B) Dynamic frequency of storage modulus (G', triangle) and the loss modulus (G'', circle) of **gel 2** (black) and **gel 2-D** (red) at the strain of 1.0% and 25 °C. (C) HPLC traces of **gel 2** (black), **gel 2-D** (red), **1** (blue), and **2** (green). Wavelength for detection: 320 nm. (D) High-resolution electrospray ionization mass spectrum of the **2-D** peak at the retention time of 12.3 min in the red HPLC trace in (C). Inset shows the structural model of **2-D** in which red represents O atom, blue represents N atom, and yellow represents S atom.

tion groups was synthesized with solid-phase peptide synthesis, and coupling of **1a** with CBT yielded **1b** and deprotection of **1b** yielded **1** after high-performance liquid chromatography (HPLC) purification. **2** was synthesized with the above procedure by using Boc-Cys(SEt)-Glu(OtBu)-Tyr(OtBu)-Phe-Phe-Gly-OH (**2a**) as the starting material. After **1** and **2** were fully characterized (Figures S1−S6), we first tested their feasibility of self-assembling into nanofibers to form hydrogels. Dissolving 2.0 mg of **1** in 200 μL phosphate buffer (0.2 M, pH 7.4) in a vial resulted in a relatively clear solution of **1** at 1.0 wt % (left photo in Figure S7). After the **1** solution was added with 40 units of ALP and incubated for 2 h at 37 °C, it turned to a light-yellow turbid hydrogel **gel 2** in the vial (left photo in Figure 2A), suggesting **1** was dephosphorylated by ALP to yield hydrogelator **2** which self-assembled into nanofibers in the hydrogels. Interestingly, directly dissolving 2.0 mg **2** in 200 μL phosphate buffer resulted in a turbid solution, and applying the solution with a heat up-cool down process did not lead to the formation of **gel 2** (data not shown). This indicated that compound **2** itself was not a good hydrogelator. After the first-order self-assembly, we added 5 μL GSH in phosphate buffer (5 equiv of **1**) to the above **gel 2** and incubated the hydrogel at 37 °C for 2 h. We found that the color of **gel 2** turned to dark-yellow, and the hydrogel became stiffer (right vial in Figure 2A). This suggests that, under GSH-reduction, **gel 2** evolved into new hydrogel **gel 2-D**. This is because, in principle, compound **2** can be subjected to a reduction-controlled condensation reaction to yield **2-D**, which is responsible for the second-order self-assemble of nanofibers in the hydrogel. After the validation of the sequential two orders of self-assembly (i.e., ALP-catalyzed self-assembly of **gel 2** followed by GSH-controlled self-assembly of **gel 2-D**), we found that the self-assembling order was not vice versa. In detail, as shown in Figure S7, either direct incubation of above phosphate buffer solution **1** (at 1.0 wt %) with GSH (5 equiv of **1**) or further addition of ALP to above incubation mixture did not result in any hydrogelation. This result implied that our precursor **1** could only be subjected to hierarchical self-assemblies to form nanofibers from extracellular environment to intracellular environment but not vice versa.

To further evaluate the hierarchical self-assemblies of nanofibers in **gel 2** and **gel 2-D**, we studied the viscoelastic properties of the hydrogels. First, dynamic strain sweep was employed to determine the proper condition for the dynamic frequency sweep of the hydrogels. As shown in Figure S8, the values of the storage modulus (G') and the loss modulus (G'') of both **gel 2** and **gel 2-D** exhibit a weak dependence from 0.01% to

DOI: 10.1021/jacs.6b06903
J. Am. Chem. Soc. 2016, 138, 11128−11131

10.0% of strain (with G' dominating G''), indicating the formation of hydrogels. After setting the strain amplitude at 1.0% (within the linear response regime of strain amplitude), we used dynamic frequency sweep to study the rheology of **gel 2** and **gel 2-D**. As shown in Figure 2B, the G' and G'' of **gel 2** and **gel 2-D** slightly increase with the increase of frequency from 0.01 to 10 Hz. The values of G' are about 5 times larger than those of G'' in this range (0.01−10 Hz), suggesting that **gel 2** and **gel 2-D** are fairly tolerant to external shear force. Moreover, the G' and G'' values of **gel 2-D** are 10 times larger than those of **gel 2**, respectively, suggesting that **gel 2-D** is mechanically stronger than **gel 2** and more tolerant to external force. This might be explained that, compared with the linear $\pi-\pi$ stacking of **2** in the first-order self-assembly, the formation of the cyclic hydrogelator **2-D** greatly enhanced the $\pi-\pi$ stacking in the second-order self-assembly, as illustrated in Figure 1.

To chemically characterize the composition of the hydrogels, we directly dissolved **gel 2** and **gel 2-D** in 30% CH_3CN in water and injected the mixture into a HPLC system for analysis. HPLC trace of **gel 2** showed that, besides the peak of precursor **1** at retention time of 13.8 min (40.4%), a new peak at retention time of 16.9 min (59.6%), whose high-resolution mass spectrum indicates the structure of **2** (Figures S9), appeared (Figure 2C). This indicated that most of precursor **1** in **gel 2** was efficiently converted to **2** by ALP. HPLC trace of **gel 2-D** showed that the main components of **gel 2-D** were **2-D** (56.5%) (Figures 2D and S10) and the cyclized dimer of **1** (i.e., **1-D**, Figure S11) (26.0%) at retention times of 12.3 and 8.5 min, respectively (Figure 2C). This indicated that **1** and **2** in **gel 2** were cleanly converted to **1-D** and **2-D** in **gel 2-D** by GSH-controlled condensation, respectively. Although the hierarchical self-assemblies were not reversible (i.e., transition from **gel 2-D** to **gel 2** was impractical) as mentioned above, the chemical evolution from **1** to **2-D**, however, could be realized by sequential treatment of **1** with GSH and ALP (i.e., formation of **1-D** first then the formation of **2-D**) (Figure S12).

To investigate the morphologies of the nanofibers in **gel 2** and **gel 2-D**, we performed cryo transmission electron microscopy (cryo-TEM) observations. The microscopic structure of **gel 2** at 1.0 wt % under cryo-TEM exhibited short and sparse nanofibers with an average width of 4.21 ± 0.48 nm (Figures 3A and S13). A cryo-TEM image of **gel 2-D** at 1.0 wt % showed longer and more condensed nanofibers than those observed in **gel 2**, with an average width of 4.03 ± 0.35 nm (Figures 3B and S14). The difference of the fiber length and density between their nanofibers well explained the mechanical difference between these two hydrogels (i.e., **gel 2-D** was mechanically stronger than **gel 2**). This also implied that the hydrogelator **2-D** is more prone to self-assembling than **2**, suggested by a lower critical micelle concentration 4.56 μM of **2-D** than that 23.4 μM of **2** in phosphate buffer (Figure S15).

To further understand the molecular packing in the nanofibers, we obtained the circular dichroism (CD) spectra of **gel 2** and **gel 2-D**. As shown in Figure S16, a negative Cotton effect at 223 nm for **gel 2** indicated that the molecule **2** may adopt β-sheet-like secondary structure.[28] CD spectrum of **gel 2-D** exhibited two negative peaks at 245 and 255 nm, indicating the chiral arrangement of the aromatic side chains of **2-D**.[27] CD spectra in the UV−vis region (>300 nm) of **gel 2** and **gel 2-D** suggested the different chiral arrangements of the chromophore CBT and luciferin in their respective fiber aggregates and totally different tertiary structures between these two gels.[29] Fluorescence emission spectra of solution **1**, **gel 2**, and **gel 2-D**

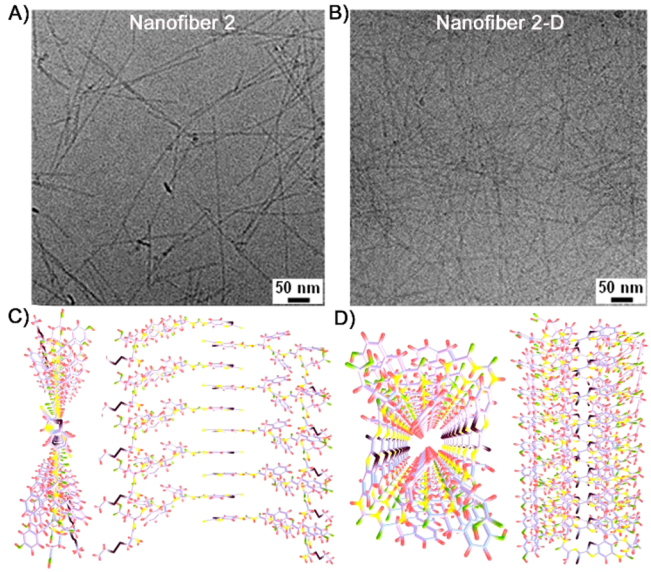

Figure 3. Cryo-TEM images of the nanofibers in **gel 2** (A) and **gel 2-D** (B) at 1.0 wt %. The proposed molecular arrangements of **2** in **nanofiber 2** (C) and **2-D** in **nanofiber 2-D** (D). Top (left) and side (right) views.

indicated that while solution **1** showed an emission peak at about 420 nm, **gel 2** and **gel 2-D** exhibited red-shifted and broadened emission peaks at about 433 and 453 nm, respectively (Figure S17), suggesting efficient stacking of the chromophores in their corresponding hydrogels.

Based on the cyro-TEM and spectroscopic results, the molecular packings of nanofiber **2** and **2-D**, driven by $\pi-\pi$ stacking among the aromatic rings, were proposed and shown in Figure 3C,D. For **nanofiber 2**, the aromatic CBT motifs in molecule **2** stack layer by layer with each neighboring CBT motif being positioned in the opposite direction to form the hydrophobic inner layer. From this molecular arrangement model, the **nanofiber 2** has a calculated diameter of 4.40 nm, in good agreement with the cryo-TEM observation (i.e., 4.21 nm). For **nanofiber 2-D**, the amphiphilic cyclic structures of the dimeric molecule (i.e., **2-D**) stack layer by layer, of which the aromatic luciferin motifs and the phenyl groups are stacked in the same direction to offer the strong $\pi-\pi$ stacking interactions. From this model, the **Nanfiber 2-D** has a calculated diameter of 4.07 nm, also in good agreement with the cryo-TEM observation (i.e., 4.03 nm).

After in vitro validation of the hierarchical self-assembly of nanofibers, we then verified whether the precursor **1** could differentiate cell environments and transform to different desired hydrogelators as proposed. Starved HeLa cells were incubated with 200 μM **1** in the culture medium at 37 °C for 4 h and then lysed. The cell lysate, together with the culture medium, was injected into a HPLC system for analysis. As shown by the HPLC traces in Figure S18, in the extracellular environment, 95.5% of the precursor **1** was dephosphorylated to yield **2** by the surface and secretory ALP in the pericellular space. In the intracellular environment, the GSH-controlled condensation product of **2** (i.e., **2-D**, 87.3%), as the main product, appeared in the trace. To further confirm the working principle, we separately used ALP inhibitor complex II (Sangon Biotech, China) or H_2O_2 as the scavenger against glutathione to pretreat the HeLa cancer cells before incubating the cells with **1**. For the ALP inhibitor experiment, as shown in Figure S18, the dephosphorylation product of **1** (i.e., **2**) decreased to 26.9% in the extracellular

DOI: 10.1021/jacs.6b06903
J. Am. Chem. Soc. 2016, 138, 11128−11131

environment. Unanimously, in the intracellular environment, GSH-controlled condensation product of **1** (i.e., **1-D**, 79.2%) appeared as the main product. For the H_2O_2-pretreated HeLa cells incubated with **1**, their HPLC traces became more complex. However, the efficient cleavage of the phosphate group of **1** to yield the hydrogelator **2** (84.6%) in the extracellular environment could still be observed, and due to the depletion of GSH by H_2O_2, **1-D** and **2-D** in the intracellular environment only, respectively, accounted for 6.6% and 23.7% of the four compounds, suggesting that **1** and **2** were not effectively reduced by GSH. Compound distribution in different cell environments calculated from the HPLC peak areas in Figure S18 is summarized in Tables S1 and S2. Cryo-TEM observations were conducted after the cells were incubated with 1.0 mM **1** at 37 °C for 4 h. The medium containing the pericellular hydrogel was collected, whose cryo-TEM image confirmed the presence of nanofibers with an average width of 4.40 ± 0.28 nm (Figure S19). The collected cells were lysed in phosphate buffer (0.2 M, pH 7.4) by ultrasound, and the resulting suspension clearly showed the existence of nanofibers with an average width of 4.26 ± 0.46 nm under cryo-TEM (Figure S20). These results of real cell samples echoed the in vitro results that **1** could differentiate cell enivironments to self-assemble into different nanofibers.

In summary, we have rationally designed a precursor **1**, which can efficiently yield amphiphilic hydrogelators **2** and **2-D** to form their corresponding hydrogels under the sequential treatment of ALP and GSH. Rheology studies indicated that **gel 2-D** was mechanically stronger than **gel 2** and cryo-TEM images showed that **gel 2-D** has longer and denser nanofibers than **gel 2**. Molecule arrangements indicated that **nanofiber 2-D** and **nanofiber 2** have totally different molecule packing models. Since the extracellualr environment of some cancer cells contains a large amount of ALP while their intracellular environment is GSH-abundant, our precursor **1** could differentiate the cell environments to self-assemble into different nanofibers. This was verified by HPLC analyses and cyro-TEM observations of the culture medium and the lysate of the cells incubated with **1**. We envision that, by employing a click condensation reaction, this work offers a platform for facile postmodulation of supramolecular nanofibers, and the versatile precursor **1** could be used to kill two birds with one stone.

■ ASSOCIATED CONTENT

Supporting Information

The Supporting Information is available free of charge on the ACS Publications website at DOI: 10.1021/jacs.6b06903.

Experimental details and data (PDF)

■ AUTHOR INFORMATION

Corresponding Author

*gliang@ustc.edu.cn

Notes

The authors declare no competing financial interest.

■ ACKNOWLEDGMENTS

This work was supported by Collaborative Innovation Center of Suzhou Nano Science and Technology, the Major program of Development Foundation of Hefei Center for Physical Science and Technology, Hefei Science Center CAS (2015HSC-UP012), and the National Natural Science Foundation of China (grants U1532144 and 21375121).

■ REFERENCES

(1) Fan, H. H.; Yan, G. B.; Zhao, Z. L.; Hu, X. X.; Zhang, W. H.; Liu, H.; Fu, X. Y.; Fu, T.; Zhang, X. B.; Tan, W. H. *Angew. Chem., Int. Ed.* **2016**, *55*, 5477.
(2) Deng, R. R.; Xie, X. J.; Vendrell, M.; Chang, Y. T.; Liu, X. G. *J. Am. Chem. Soc.* **2011**, *133*, 20168.
(3) Banerjee, R. *J. Biol. Chem.* **2012**, *287*, 4397.
(4) Filomeni, G.; Rotilio, G.; Ciriolo, M. R. *Biochem. Pharmacol.* **2002**, *64*, 1057.
(5) Tate, S. S.; Grau, E. M.; Meister, A. *Proc. Natl. Acad. Sci. U. S. A.* **1979**, *76*, 2715.
(6) Rahman, I.; Kode, A.; Biswas, S. K. *Nat. Protoc.* **2006**, *1*, 3159.
(7) Jung, H. S.; Chen, X. Q.; Kim, J. S.; Yoon, J. *Chem. Soc. Rev.* **2013**, *42*, 6019.
(8) Yuan, Y.; Zhang, J.; Wang, M.; Mei, B.; Guan, Y.; Liang, G. *Anal. Chem.* **2013**, *85*, 1280.
(9) Niu, L. Y.; Guan, Y. S.; Chen, Y. Z.; Wu, L. Z.; Tung, C. H.; Yang, Q. Z. *J. Am. Chem. Soc.* **2012**, *134*, 18928.
(10) Yang, C.; Wang, Z.; Ou, C.; Chen, M.; Wang, L.; Yang, Z. *Chem. Commun.* **2014**, *50*, 9413.
(11) Wang, H.; Mao, D.; Wang, Y.; Wang, K.; Yi, X.; Kong, D.; Yang, Z.; Liu, Q.; Ding, D. *Sci. Rep.* **2015**, *5*, 16680.
(12) Yang, C. H.; Li, D. X.; Liu, Z.; Hong, G.; Zhang, J.; Kong, D. L.; Yang, Z. M. *J. Phys. Chem. B* **2012**, *116*, 633.
(13) Ma, C.; Shi, Y.; Pena, D. A.; Peng, L.; Yu, G. H. *Angew. Chem., Int. Ed.* **2015**, *54*, 7376.
(14) Maity, C.; Hendriksen, W. E.; van Esch, J. H.; Eelkema, R. *Angew. Chem., Int. Ed.* **2015**, *54*, 998.
(15) Alonso, A.; Sasin, J.; Bottini, N.; Friedberg, I.; Friedberg, I.; Osterman, A.; Godzik, A.; Hunter, T.; Dixon, J.; Mustelin, T. *Cell* **2004**, *117*, 699.
(16) Filipponi, D.; Muller, J.; Emelyanov, A.; Bulavin, D. V. *Cancer Cell* **2013**, *24*, 528.
(17) Iantomasi, T.; Favilli, F.; Catarzi, S.; Giannoni, E.; Biagioni, C.; Vincenzini, M. T. *IUBMB Life* **2003**, *55*, 159.
(18) de la Croix Ndong, J.; Makowski, A. J.; Uppuganti, S.; Vignaux, G.; Ono, K.; Perrien, D. S.; Joubert, S.; Baglio, S. R.; Granchi, D.; Stevenson, D. A.; Rios, J. J.; Nyman, J. S.; Elefteriou, F. *Nat. Med.* **2014**, *20*, 904.
(19) Gao, Y.; Shi, J.; Yuan, D.; Xu, B. *Nat. Commun.* **2012**, *3*, 1033.
(20) Wu, C. C.; Hsu, C. W.; Chen, C. D.; Yu, C. J.; Chang, K. P.; Tai, D. I.; Liu, H. P.; Su, W. H.; Chang, Y. S.; Yu, J. S. *Mol. Cell. Proteomics* **2010**, *9*, 1100.
(21) Zhou, J.; Du, X.; Yamagata, N.; Xu, B. *J. Am. Chem. Soc.* **2016**, *138*, 3813.
(22) Yang, Z.; Liang, G.; Guo, Z.; Guo, Z.; Xu, B. *Angew. Chem., Int. Ed.* **2007**, *46*, 8216.
(23) Ren, C. H.; Wang, H. M.; Mao, D.; Zhang, X. L.; Fengzhao, Q. Q.; Shi, Y.; Ding, D.; Kong, D. L.; Wang, L.; Yang, Z. M. *Angew. Chem., Int. Ed.* **2015**, *54*, 4823.
(24) Liang, G.; Ronald, J.; Chen, Y.; Ye, D.; Pandit, P.; Ma, M. L.; Rutt, B.; Rao, J. *Angew. Chem., Int. Ed.* **2011**, *50*, 6283.
(25) Ai, X. Z.; Ho, C. J. H.; Aw, J.; Attia, A. B. E.; Mu, J.; Wang, Y.; Wang, X. Y.; Wang, Y.; Liu, X. G.; Chen, H. B.; Gao, M. Y.; Chen, X. Y.; Yeow, E. K. L.; Liu, G.; Olivo, M.; Xing, B. G. *Nat. Commun.* **2016**, *7*, 10432.
(26) Liu, S.; Tang, A.; Xie, M.; Zhao, Y.; Jiang, J.; Liang, G. *Angew. Chem., Int. Ed.* **2015**, *54*, 3639.
(27) Liu, S.; Luo, Y.; Liang, G. *Nanoscale* **2016**, *8*, 766.
(28) Greenfield, N. J. *Nat. Protoc.* **2006**, *1*, 2876.
(29) Yoshii, T.; Ikeda, M.; Hamachi, I. *Angew. Chem., Int. Ed.* **2014**, *53*, 7264.

■ NOTE ADDED AFTER ASAP PUBLICATION

This paper was published ASAP on August 25, 2016. The chemical structure for compound 2 in Figure 1 was incorrect. Figure 1 has been updated and the revised version was posted on September 7, 2016.

DOI: 10.1021/jacs.6b06903
J. Am. Chem. Soc. 2016, 138, 11128−11131